Perturbation model to predict the effect of spatially varying absorptive inhomogeneities in diffusing media

S. De Nicola
Istituto Nazionale di Ottica Applicata, Sez. di Napoli, e/o Istituto di Cibernetica del C.N.R. "E. Caianiello," compr. A. Olivetti, Via Campi Flegrei 34, 80078 Pozzuoli, Italy

R. Esposito
Dipartimento Scienze Fisiche – Università "Federico II," Napoli, Italy
and Istituto Naziarale di Fisica della Materia, Unità di Napoli, Napoli, Italy

M. Lepore
Dipartimento di Medicina Sperimentale, Seconda Università di Napoli, Napoli, Italy
(Received 24 April 2003; published 1 August 2003)

We develop a perturbation model to predict the effect of a spatially varying absorptive inhomogeneities in a diffusing slab. The model is based on a perturbation solution of diffusion equation derived for a refractive index mismatch between the scattering slab and the surrounding medium, through the use of the extrapolated boundary conditions. We show that the model allows to compute the time-dependent relative change in the transmitted signal resulting from the presence of the inclusion. We derive simplified expressions for the perturbed time-resolved transmittance that allows to implement an efficient fitting procedure for obtaining the optical properties of the absorptive inclusion. The accuracy of the predictions of the model was investigated through comparison with the results of the Finite Element Method to solve the time-dependent diffusion equation numerically. The procedure is used to obtain the absorption perturbation parameter of an absorptive inclusion characterized by spatially dependent Gaussian distribution of its absorption coefficient located at the midplane of a scattering slab.

DOI: 10.1103/PhysRevE.68.021901 PACS number(s): 87.10.+e, 42.25.Dd, 42.62.Be

I. INTRODUCTION

The study of light propagation through highly scattering media is a topic of a rapidly growing research area, especially in the framework of biomedical applications [1–4]. This has been motivated by the fact that imaging through tissues using light in the near infrared spectral region is characterized by a penetration capability of several centimeters due to the low absorption of the tissues [5,6]. As an ultrashort laser light pulse enters a slab of scattering material, such as a thick tissue, the phase and polarization of the propagating electromagnetic field are randomized because of scattering and they lose their physical relevance. Therefore, a more suitable description based only on the energetic aspects accounts for the photon migration through the medium [7]. Such a description relies on a radiative transfer equation that considers the spatial redistribution of the light irradiance inside the medium. The radiative transfer equation cannot be solved analytically in a closed form, but it can be made more tractable through various approximations [8]. Of these approximations, the most widely used in the field of bio-optics and in imaging in optically thick tissues assumes that the photon fluence rate, i.e., the local photon density, be described by a time-dependent diffusion equation [9]. An important application is the optical tomography in medical imaging, such as breast cancer detection, in which time-resolved techniques are used to produce imaging in highly scattering media [4,10]. Analytical expressions for the time-resolved transmittance and reflectance have been obtained [11,12] for simple geometries such as an infinitely extended slab of a given thickness, for the particular case of a homogeneous scattering medium. Expressions have also been derived for the perturbation on the diffuse reflectance and transmittance caused by a small inclusion with a spatially uniform optical properties differing slightly from those of the host medium [13–17]. It has been shown [18,19] that the results for this simple geometry are of valuable practical interest, inasmuch as the diffusion equation is an adequate model for the photon density distribution. Indeed, to be of practical interest, any approximate perturbation-based scheme for image reconstruction has to predict, as accurate as possible, the effect of the inhomogeneities that cause perturbation on photon migration in an otherwise homogeneous unperturbed medium. The basic purpose of a perturbation model is to provide an efficient curve-fitting procedure to output the parameters of the analytical solution and, in particular, the optical coefficients of the inclusion as well as their spatial distribution over the probed region, which is a significant task for tissue type recognition. In principle, the prediction of perturbation model is expected to give accurate results when the effect of the inclusion on photon migration is smaller. This means that differences of the optical coefficients of the inclusion with respect to the surrounding medium and the volume of the inhomogeneity are small. Consequently, it is important to develop a perturbation model that takes into account the effect of spatially varying optical parameters of the inclusion and to investigate the accuracy of the model when the volume of the inclusion cannot be neglected even if we limit to a first-order approximation perturbation scheme.

Our purpose is to develop a consistent perturbation model that accounts for the effect of spatially varying optical parameters of an absorptive inclusion and to better understand the limitations of the small volume approximation on the perturbed time-resolved transmittance. This model is expected to be more effective in the realistic case of imaging reconstruction of inclusions whose optical properties change continuously going from the region of the anomalous defect to the surrounding normal tissue.

In Sec. II we will asses the problem and consider the case of spatially dependent Gaussian distributed absorptive inclusion embedded in a thick diffusing slab, in coaxial probe beam-detector configuration. We will show that for this model, it is possible to arrive at particularly simple expressions to describe the change in the time-resolved transmittance resulting from the presence of the inclusion; expressions of the time-resolved contrast functions are derived for a refractive-index mismatch between the scattering slab and the surrounding medium by using the extrapolated boundary conditions.

The simplicity of the perturbed expressions allows for a fast and reliable implementation of a fitting procedure for recovering the optical parameters of the absorptive inhomogeneity. This is of particular significance in optical detection of absorptive inclusions such as the case of many kinds of tumors in near infrared [20]. In Sec. III the time-resolved contrast function computed by the perturbation model have been compared with that obtained by the Finite Element Method (FEM) simulations to solve the time-dependent diffusion equation numerically in presence of the spatially varying absorptive inclusion. In Sec. IV we have developed a detailed quantitative investigation of the accuracy of the predictions and of the application range of the proposed model through comparison of the perturbed time-resolved transmittance with that obtained by the FEM. The FEM calculations are used to validate the perturbed model by determining the relative error of the fitting procedure for obtaining the absorption perturbation parameter of the inclusion for different optical parameters of the host medium and of the size of the inhomogeneity.

II. THEORY

A. Homogeneous slab solution

Let us consider an infinitely extended homogeneous slab with thickness d, absorption and the reduced scattering coefficients μ_a and μ_s', respectively, and diffusion coefficient $D=1/3\mu_s'$. Within the diffusion approximation, when a pulsed laser beam hits normally upon the surface of the slab, the temporal and spatial distribution of the light can be derived by assuming that all photons are initially isotropically scattered at a depth $z=1/\mu_s'$ below the surface. With reference to Fig. 1, the isotropic pointlike source $S(\mathbf{r},t;\mathbf{r_s},t_s)=\delta(\mathbf{r}-\mathbf{r_s})\delta(t-t_s)/4\pi$ is located at $\mathbf{r_s}=(x_s,y_s,z_s=1/\mu_s')$ and emits a pulse of unit energy at time $t=t_s$.

The light propagates in the medium undergoing many scattering events and its density photon fluence rate $\Phi(\mathbf{r},t;\mathbf{r_s},t_s)$ at position $\mathbf{r}=(x,y,z)$ and time t is described

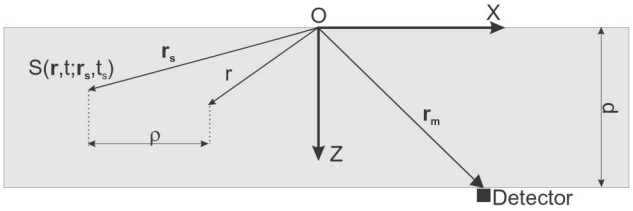

FIG. 1. Geometric scheme of an infinitely extended homogeneous slab.

by the following parabolic differential equation:

$$\left[D\nabla^2-\frac{1}{v}\frac{\partial}{\partial t}-\mu_a\right]\Phi(\mathbf{r},t;\mathbf{r_s},t_s)=-S(\mathbf{r},t;\mathbf{r_s},t_s), \quad (1)$$

where v is the speed of light in the medium. The general solution (Green's function) of Eq. (1) for an isotropic source in an infinitely extended homogeneous scattering and absorbing medium is given by

$$\Phi_G(\mathbf{r}-\mathbf{r_s},t-t_s)=\frac{v\exp\left[-\mu_a v(t-t_s)-\dfrac{|\mathbf{r}-\mathbf{r_s}|^2}{4Dv(t-t_s)}\right]}{[4\pi Dv(t-t_s)]^{3/2}}. \quad (2)$$

In order to describe the internal redistribution of light due to the Fresnel reflections at the slab interfaces, we have to consider the relative refractive index n, i.e., the ratio between the refractive index of the scattering medium and that of the external one. It has been shown [21–23] that the two mismatched boundaries can be described by the following two expressions, namely:

$$\Phi(x,y,z=0,t;\mathbf{r_s},t_s)=z_e\frac{\partial\Phi}{\partial z}(x,y,z,t;\mathbf{r_s},t_s)\big|_{z=0}, \quad (3a)$$

$$\Phi(x,y,z=d,t;\mathbf{r_s},t_s)=-z_e\frac{\partial\Phi}{\partial z}(x,y,z,t;\mathbf{r_s},t_s)\big|_{z=d}. \quad (3b)$$

The quantity z_e in Eqs. (3) is the so-called extrapolated distance, and is given by the simple relation $2A(n)D$, where the coefficient $A(n)$ takes into account the effects of the Fresnel reflections at the two interfaces and can be obtained through a seven-order polynomial approximation in terms of the relative refractive index n [23]. For example, if we consider a relative refractive index of $n=1.4$ [24] the corresponding value of the coefficient $A(n)$ is 2.95 and the distance z_e between the extrapolated boundaries and the surfaces of the slab is $z_e=5.88D=1.97/\mu_s'$. A further approximation is commonly used to solve Eq. (1) together with the boundary conditions given by Eqs. (3), according to which the fluence rate is set to 0 at the two extrapolated boundaries $z=-z_e$ and $z=d+z_e$, i.e., one assumes

$$\Phi(x,y,z=-z_e,t;\mathbf{r_s},t_s)=0,$$

$$\Phi(x,y,z=d+z_e,t;\mathbf{r_s},t_s)=0. \quad (4)$$

The expression for the fluence rate $\Phi(\mathbf{r},t;\mathbf{r_s},t_s)$, which satisfies the extrapolated boundary conditions given by Eq. (4), is obtained [23] by using the basic isotropic solution (2) and by adding an infinite number of dipoles located along the z axis, representing pairs of negative and positive pointlike sources, namely,

$$\Phi(\mathbf{r},t;\mathbf{r_s},t_s)=\frac{v\exp\left[-\mu_a v(t-t_s)-\frac{\rho^2}{4Dv(t-t_s)}\right]}{4\pi[4Dv(t-t_s)]^{3/2}} \times\sum_{m=-\infty}^{\infty}\left\{\exp\left[-\frac{(z-z_{+m})^2}{4\pi Dv(t-t_s)}\right] -\exp\left[-\frac{(z-z_{-m})^2}{4\pi Dv(t-t_s)}\right]\right\}, \tag{5}$$

where ρ is the radial distance between positions $\mathbf{r}$ and $\mathbf{r_s}$; the quantities z_{+m} and z_{-m} given by

$$z_{+m}=2md_e+z_s,$$
$$z_{-m}=2md_e-2z_e-z_s, \tag{6}$$

define the locations of the positive and negative pointlike sources along the z axis, and $d_e=d+2z_e$ is the extrapolated thickness of the slab. In the following we will recast Eq. (5) for the fluence rate in a different form which will result in a more amenable and compact expression for the time-resolved transmittance T_{pert} when an inhomogeneity is present. For the purpose we make use of the following Poisson summation formula, namely:

$$\frac{1}{\sqrt{t}}\sum_{m=-\infty}^{\infty}\exp\left[-\frac{\pi(z+m)^2}{t}\right] =\sum_{m=-\infty}^{\infty}\exp[-m^2\pi t-i2m\pi z]. \tag{7}$$

By using the above formula into Eq. (5), after somewhat lengthy but straightforward algebra we obtain the following expression for the fluence rate $\Phi(\mathbf{r},t;\mathbf{r_s},t_s)$:

$$\Phi(\mathbf{r},t;\mathbf{r_s},t_s)=\frac{\exp\left[-\mu_a v(t-t_s)-\frac{\rho^2}{4Dv(t-t_s)}\right]}{8\pi^2 Dd_e(t-t_s)} \times\sum_{m=1}^{\infty}\exp\left[-\frac{\pi^2m^2Dvt'}{d_e^2}\right]\sin\left(\frac{m\pi(z_s+z_e)}{d_e}\right) \times\sin\left(\frac{m\pi(z+z_e)}{d_e}\right). \tag{8}$$

Equation (8) is basically a Fourier series development of the fluence rate and it is easy to see that each term of this series satisfies the extrapolated boundary conditions given by Eq. (4). Although Eq. (8) for the fluence rate is the Poisson sum corresponding to Eq. (5), it can be derived quite straightforwardly by applying to Eq. (1) the separation of variables.

The physical quantity of interest is the transmittance T through the slab, given by the Fick law,

$$T(\mathbf{r_m},t;\mathbf{r_s},t_s)=-4\pi D\frac{\partial\Phi}{\partial z}(\mathbf{r_m},t;\mathbf{r_s},t_s)\big|_{z_m=d}, \tag{9}$$

where $\mathbf{r_m}=(x_m,y_m,d)$ is a measurement point on the $z=d$ surface at time t (see Fig. 1). If we take into account boundary condition (3b), we can express the transmittance $T(\mathbf{r_m},t;\mathbf{r_s},t_s)$ directly in terms of the fluence rate $\Phi(\mathbf{r},t;\mathbf{r_s},t_s)$ in the following form:

$$T(\mathbf{r_m},t;\mathbf{r_s},t_s)=\frac{2\pi}{A(n)}\Phi(\mathbf{r_m},t;\mathbf{r_s},t_s), \tag{10}$$

where the $\Phi(\mathbf{r_m},t;\mathbf{r_s},t_s)$ is given by the previously derived Eq. (8).

Equation (4) for the fluence rate describes the basic solution of the homogeneous slab problem and will be used in the following for calculating the first-order perturbed time-resolved transmittance.

B. Gaussian absorptive inclusion

Localized slight changes in optical properties of an homogeneous turbid medium result in a change in the photon fluence rate and, consequently, in the time-resolved transmittance. The analytical solution of the diffusion equation that accounts for the effect of an inclusion on the light propagation in a turbid medium cannot be obtained, in general. However, under the condition $|\delta\Phi|\ll\Phi$, within the Born approximation, changes in absorption and scattering affect the fluence rate linearly and independently. The change in the photon fluence rate $\delta\Phi$ can be shown to be equal to [25]

$$\delta\Phi(\mathbf{r},t)=\delta\Phi_{\mu_a}(\mathbf{r},t)+\delta\Phi_{\mu_s'}(\mathbf{r},t), \tag{11}$$

where $\delta\Phi_{\mu_a}(\mathbf{r},t)$ describes the effect of an absorptive inclusion on the light distribution within an otherwise homogeneous medium and, similarly, $\delta\Phi_{\mu_s'}(\mathbf{r},t)$ describes the perturbation to the photon density due to a diffusive inclusion. Let us consider the injection of a pulsed laser beam into a slab of turbid medium in which an inclusion is to be detected in a coaxial measurement arrangement. This measurement scheme has been employed for inclusion characterization in a turbid slab with time-resolved transmittance measurements. Furthermore, general time-domain expressions for the perturbation of the light transmittance that results from localized slight changes in absorption and scattering coefficients of the turbid slab have been reported when the inclusion is small enough to be considered pointlike [15,16]. In this scheme the probe beam, the inclusion, and the detector are collinear. The situation to be considered in the following is an absorptive inclusion of cylindrical shape geometry. In Fig. 2 the inclusion is depicted as a cylinder of height h centered at $z=z_{pc}$

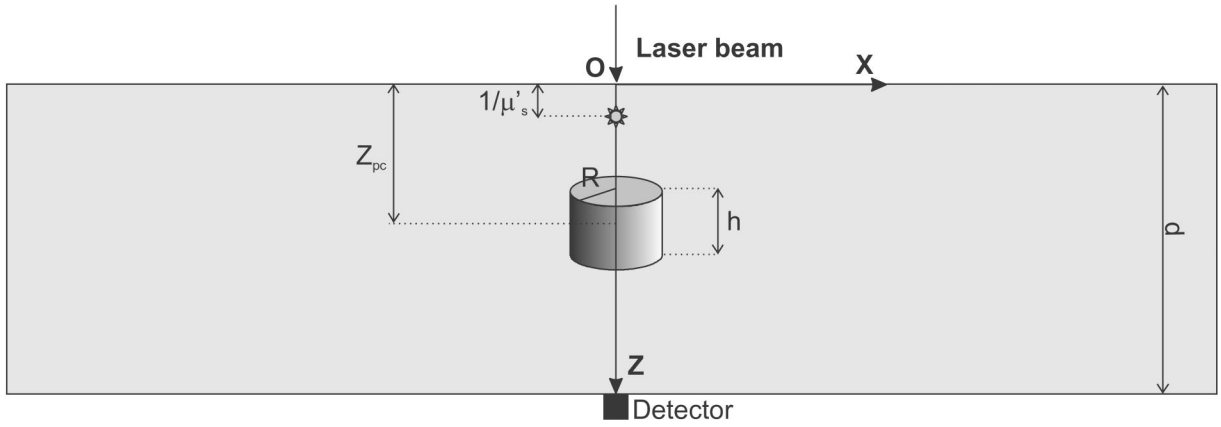

FIG. 2. Geometric scheme assumed for the perturbation model. A Gaussian absorptive inclusion of cylindrical shape geometry with radius R and height h is centred at $z=z_{pc}$ inside a turbid slab of thickness d. A pulsed light beam illuminates the front surface of the scattering slab at plane $z=0$. The time-resolved transmittance is measured by a detector at plane $z=d$ coaxial with the source and with the inclusion.

whose spatial dependent absorption coefficient is assumed to be varying along the radial distance ρ_p according to a Gaussian distribution law, namely,

$$\delta\mu_a(\mathbf{r_p})=\Delta\mu_a\exp\left[-2\ln 2\left(\frac{\rho_p}{R}\right)^2\right], \tag{12}$$

In Eq. (12) $\Delta\mu_a$ is the value of the Gaussian absorptive inclusion on the cylinder axis and corresponds to the maximum deviation of the absorption coefficient of the inclusion from the unperturbed value μ_a. The radius R that determines the radial size of the inclusion has been defined such that the value of the absorption coefficient of the inclusion decreases to $\Delta\mu_a/4$ at a distance $\rho_p=R$ from the cylinder axis. As described in the preceding section we consider a slab of thickness d containing a Dirac δ-point source located at distance $1/\mu_s'$, which emits a pulse of unit energy at time $t_s=0$. According to the first-order perturbation method [26,27], the general expression for computing the change $\delta\Phi_{\mu_a}(\mathbf{r},t)$ is given by the following:

$$\delta\Phi_{\mu_a}(\mathbf{r},t;;\mathbf{r_s},t_s=0)=-\int_0^t dt'\int\int\int d\mathbf{r_p}\delta\mu_a(\mathbf{r_p})\times\Phi(\mathbf{r},t;\mathbf{r_p},t')\Phi(\mathbf{r_p},t';\mathbf{r_s},0). \tag{13}$$

Here, the spatial integration is carried out over the region of the inclusion and the time integration goes from the initial time $t_s=0$ to the time t at which the photon density is measured. The function $\Phi(\mathbf{r},t;\mathbf{r_p},t')$ is recognizable as the Green function given by Eq. (8) where the coordinates $(\mathbf{r_s},t_s)$ of the source are replaced by $(\mathbf{r_p},t')$. Similarly, the function $\Phi(\mathbf{r_p},t';\mathbf{r_s},0)$ is the fluence rate at time t and position $\mathbf{r_p}$ of the inclusion due to a pointlike source located at position $\mathbf{r_s}$ at time $t=0$. Within the first-order approximation, the perturbed photon fluence $\Phi_{per}(\mathbf{r},t;\mathbf{r_s},t_s=0)$ is given by

$$\Phi_{per}(\mathbf{r},t;\mathbf{r_s},t_s=0)=\Phi(\mathbf{r},t;\mathbf{r_s},t_s=0)+\delta\Phi_{\mu_a}(\mathbf{r},t;;\mathbf{r_s},t_s=0), \tag{14}$$

where $\Phi(\mathbf{r},t;\mathbf{r_s},t_s=0)$ is the solution of the unperturbed problem given by Eq. (8). The corresponding perturbed time-resolved transmittance can be written in the following form

$$T_{pert}(\mathbf{r_m},t;\mathbf{r_s},t_s=0)=T(\mathbf{r_m},t;\mathbf{r_s},t_s=0)+\delta T_{\mu_a}(\mathbf{r_m},t;\mathbf{r_s},t_s=0), \tag{15}$$

where $\mathbf{r_m}$ is the measurement point. Equation (15) can be easily derived by inserting Eq. (14) for the perturbed fluence rate into the basic relationship between the time-resolved transmittance and the fluence rate given by Eq. (10). We obtain the change in the time-resolved transmittance $\delta T(\mathbf{r_m},t;\mathbf{r_s},t_s=0)$ in terms of the corresponding change in the photon fluence rate according to

$$\delta T_{\mu_a}(\mathbf{r_m},t;\mathbf{r_s},t_s=0)=\frac{2\pi}{A(n)}\delta\Phi_{\mu_a}(\mathbf{r_m},t;\mathbf{r_s},t_s=0). \tag{16}$$

Up to this point the derived expressions of $\delta\Phi_{\mu_a}$ and δT_{μ_a} are quite general within the first-order approximation theory. In the following, we employ the Gaussian absorptive inclusion model as given by Eq. (12) and determine the change δT_{μ_a} in the time-resolved transmittance in the case of the slab geometry and confocal detection arrangement schematically shown in Fig. 2. If we substitute Eqs. (12) and (8) into the perturbation integral (13) and perform the Gaussian integration over the radial coordinate ρ_p, we arrive after some manipulation at the following expression for δT_{μ_a}:

$$\delta T_{\mu_a}(z_m=d,t;z_s=1/\mu_s',t_s=0) = -\frac{\Delta\mu_a}{2A(n)\pi^2D^2d_e^2t}\sum_{k,l=1}^{\infty}\exp\left[-\mu_a v t - \frac{\pi^2 D v t(k^2+l^2)}{2d_e^2}\right]\mathcal{R}_{k,l}(R,t)\mathcal{Z}_{k,l}(z_{pc},h). \tag{17}$$

In Eq. (17) we have introduced $\mathcal{R}_{k,l}(R,t)$, which is a function of the radius R of the inclusion, namely,

$$\mathcal{R}_{k,l}(R,t) = \frac{\pi R^2 e^{-\alpha_{k,l}\beta}}{8\alpha_{k,l}\ln 2}\{[\mathrm{Ei}(\alpha_{k,l}(\beta+1)) - \mathrm{Ei}(\alpha_{k,l}(\beta-1))] + e^{2\alpha_{k,l}\beta}[\mathrm{Ei}(-\alpha_{k,l}(\beta+1)) - \mathrm{Ei}(-\alpha_{k,l}(\beta-1))]\}, \tag{18}$$

where

$$\alpha_{k,l} = \frac{\pi^2 D v t(k^2-l^2)}{2d_e^2}, \tag{19}$$

$$\beta = \sqrt{1+\frac{R^2}{2Dvt\ln 2}}, \tag{20}$$

and the exponential integral $\mathrm{Ei}(x)$ is given by

$$\mathrm{Ei}(x) = -\int_{-x}^{\infty}\frac{e^{-y}}{y}dy,$$

where the principal value of the integral is taken.

The function $\mathcal{Z}_{k,l}(z_{pc},h)$ is given by

$$\mathcal{Z}_{k,l}(z_{pc},h) = \frac{d_e}{2\pi(k^2-l^2)}\sin\left[\frac{l\pi(d+z_e)}{d_e}\right]\sin\left[\frac{k\pi(z_s+z_e)}{d_e}\right] \times\left|(k+l)\sin\left[\frac{\pi(m-n)(z_e+z)}{d_e}\right] - (k-l)\sin\left[\frac{\pi(m+n)(z_e+z)}{d_e}\right]\right|_{z=z_{pc}-h/2}^{z=z_{pc}+h/2}, \tag{21}$$

where by the notation $|\cdots|_{z=z_{pc}-h/2}^{z=z_{pc}+h/2}$ we mean the difference of the values of the function between $z=z_{pc}+h/2$ and $z=z_{pc}-h/2$. It can be verified that the general expressions for $\mathcal{R}_{k,l}(R,t)$ and $\mathcal{Z}_{k,l}(z_{pc},h)$ reduce for $k=l$ to the following form:

$$\mathcal{R}_{k,k}(R,t) = \frac{\pi R^2}{4\beta\ln 2}\ln\left(\frac{\beta+1}{\beta-1}\right), \tag{22}$$

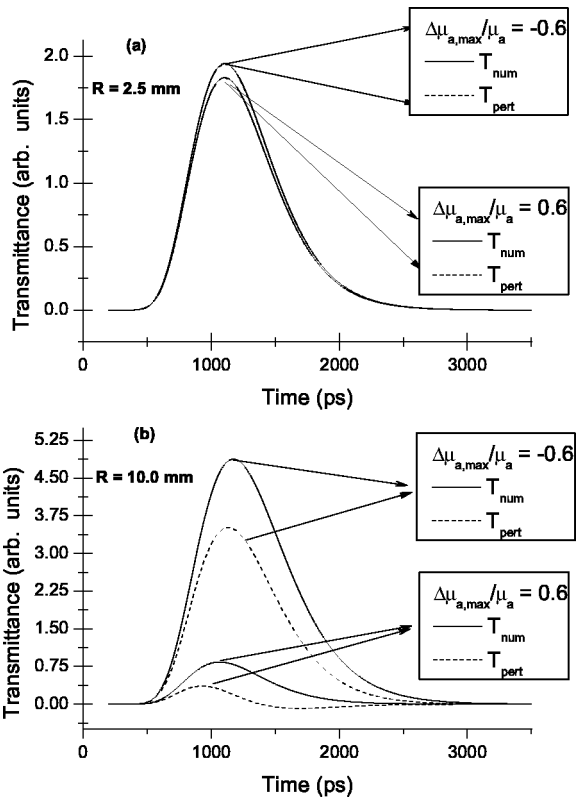

FIG. 3. Temporal profiles of the time-resolved transmittances $T_{pert}(t)$ and $T_{num}(t)$ computed by using the perturbation model and the FEM simulation, respectively, for two values of the relative absorptive perturbation parameter, $\Delta\mu_a/\mu_a=-0.6$ and $\Delta\mu_a/\mu_a=0.6$. Results refer to a turbid slab of thickness $d=40$ mm, relative refractive index $n=1.4$, absorption coefficient $\mu_a=0.02$ mm^{-1}, and reduce scattering coefficient $\mu_s'=1.5$ mm^{-1}. The inhomogeneity is located at the midplane of the slab: (a) the radius of the inclusion is $R=2.5$ mm, (b) $R=10.0$ mm.

$$\mathcal{Z}_{k,k}(z_{pc},h) = \frac{h}{2}+\frac{d_e}{4\pi k}\left\{\sin\left[\frac{\pi(m+n)\left(z_e+z_{pc}+\frac{h}{2}\right)}{d_e}\right] - \sin\left[\frac{\pi(m+n)\left(z_e+z_{pc}-\frac{h}{2}\right)}{d_e}\right]\right\}. \tag{23}$$

In the following section we will develop a thorough analysis of the perturbation model predictions based on Eq. (17).

III. DESCRIPTION OF THE NUMERICAL SIMULATIONS

The analytical solution for the change δT_{μ_a} in the time-resolved transmittance has been derived in the preceding section in the framework of the first-order perturbation approximation to the diffusion equation, in the case of a spatially varying Gaussian distributed absorptive inclusion and simple slab geometry. The perturbed solution is approximated since it has been obtained assuming that the inhomogeneity causes small perturbations on photon migration through the homo-

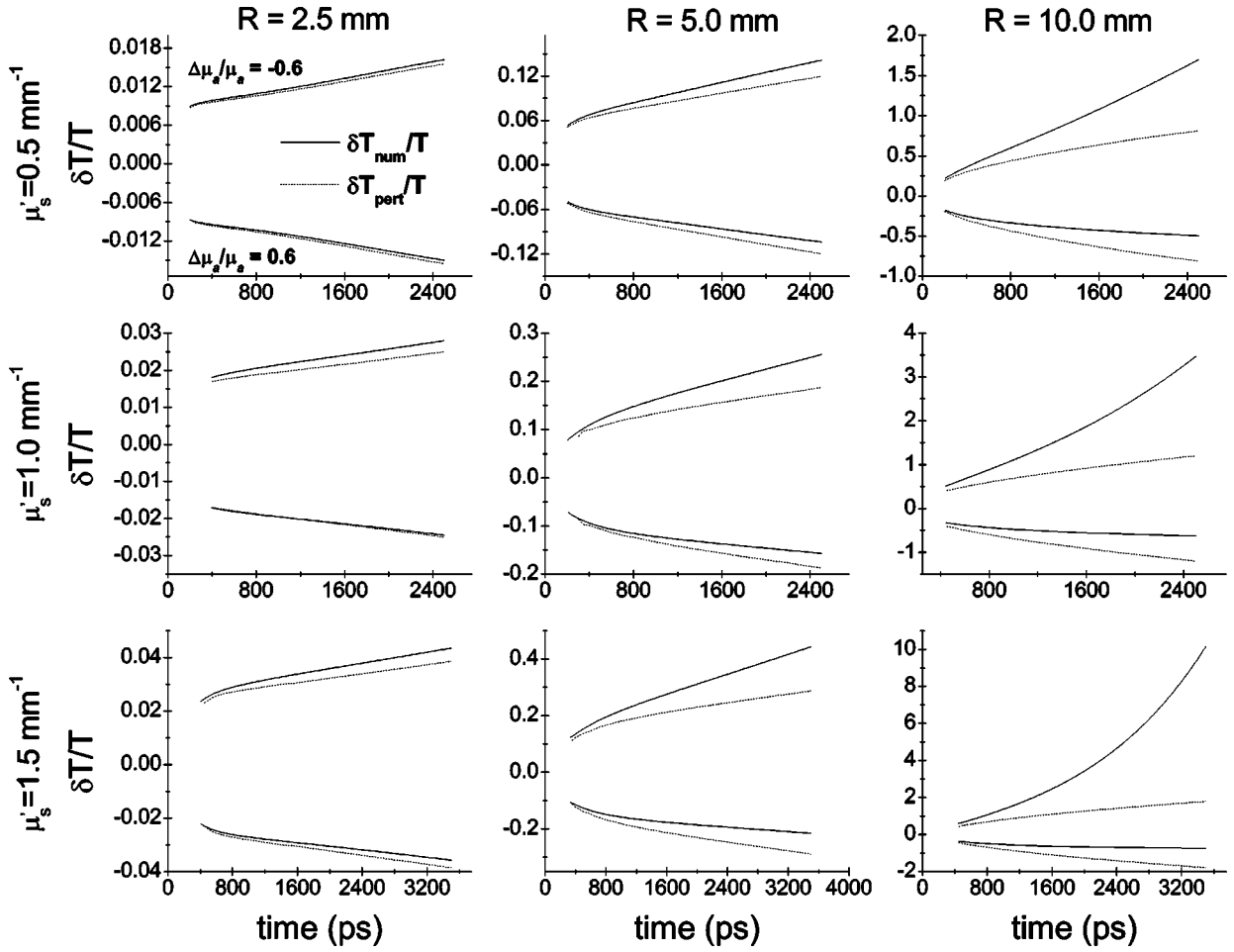

FIG. 4. Time-resolved contrast functions $\delta T_{pert}(t)/T(t)$ and $\delta T_{num}(t)/T(t)$ computed by the perturbation model and the FEM simulation, respectively, for two values of the relative absorptive perturbation, $\Delta\mu_a/\mu_a=-0.6$ and $\Delta\mu_a/\mu_a=0.6$. Row panels are obtained for the same value of the reduced scattering coefficient μ_s'; column panels are obtained for the same value of the size R of the inclusion. The other parameters are the same as of Fig. 3.

geneous medium and, consequently, it is expected to give accurate results only when local changes in the optical absorption coefficient and the size of the inhomogeneity are small with respect to the homogeneous medium. In the following, the accuracy of the perturbed transmittance $T_{pert}(t)$ is investigated through comparisons with the numerical solution $T_{num}(t)$, obtained by solving the diffusion equation for the fluence rate $\Phi_{num}(\mathbf{r},t;\mathbf{r_s},t_s=0)$ in presence of the spatially dependent absorptive inhomogeneity (12), namely,

$$\left[D\nabla^2-\frac{1}{v}\frac{\partial}{\partial t}-[\mu_a+\delta\mu_a(\mathbf{r})]\right]\Phi_{num}(\mathbf{r},t;\mathbf{r_s},t_s=0)$$
$$=-\frac{1}{4\pi}\delta(\mathbf{r}-\mathbf{r}_s)\,\delta(t), \tag{24}$$

with the two extrapolated boundary conditions

$$\Phi_{num}(x,y,z=-z_e,t;\mathbf{r_s},t_s)=0,$$
$$\Phi_{num}(x,y,z=d+z_e,t;\mathbf{r_s},t_s)=0. \tag{25}$$

The FEM has been employed to solve diffusion equation (24) under extrapolated boundary conditions (25). This method has been shown to be a robust and efficient scheme for solving the diffusion equation in the case of complex geometry and inhomogeneous media [28–30]. Figure 3 shows the temporal profiles of the time-resolved transmittances $T_{pert}(t)$ and $T_{num}(t)$ computed by using the first-order perturbation model and the FEM simulations, respectively, in the coaxial probe beam-detector configuration.

The numerical results refer to a diffusing slab of 40 mm thick. The center of the absorptive inhomogeneity is located at a depth $z_{pc}=d/2$ in the central plane of the slab, where the contrast function attains its lower value [15]. The scattering and the absorption coefficients of the unperturbed medium were assumed to be $\mu_s'=1.5\ \mathrm{mm}^{-1}$ and $\mu_a=0.02\ \mathrm{mm}^{-1}$, respectively, and the mismatch in the refractive index was set to the value 1.4. These parameters are of practical interest since they are representatives of a slightly compressed breast [16]. The comparison between the perturbation model (solids curves) and the FEM result (dashed curves) is shown in Figs. 3(a) and 3(b) for two values of the radius of the inclusion, $R=2.5$ mm and $R=10$ mm, respectively. In the numerical

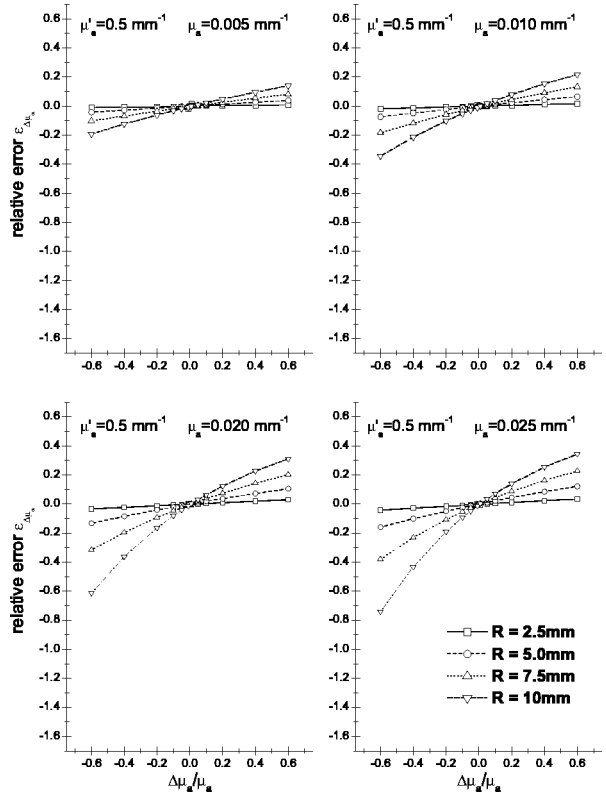

FIG. 5. Numerical calculation of the relative error $\epsilon_{\Delta\mu_a}$ as a function of the relative absorptive perturbation $\Delta\mu_a/\mu_a$ for $\mu_s'=0.5\ \mathrm{mm}^{-1}$. The four panels are obtained for increasing values (form top to bottom) of the absorption coefficient of the host medium: $\mu_a=0.005,\ 0.01,\ 0.02,\ 0.025\ \mathrm{mm}^{-1}$.

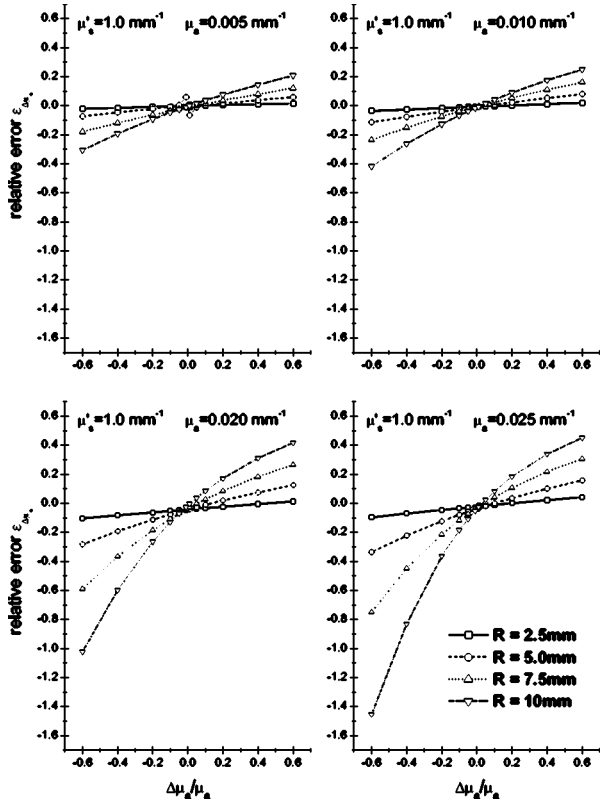

FIG. 6. Numerical calculation of the relative error $\epsilon_{\Delta\mu_a}$ as a function of the relative absorptive perturbation $\Delta\mu_a/\mu_a$ for $\mu_s'=1.0\ \mathrm{mm}^{-1}$. The four panels are obtained for increasing values (form top to bottom) of the absorption coefficient of the host medium: $\mu_a=0.005,\ 0.01,\ 0.02,\ 0.025\ \mathrm{mm}^{-1}$.

calculation, the thickness h of the cylindrical inclusion was equal to its diameter $2R$. For $R=2.5$ mm the perturbation model predictions are in excellent agreement with the FEM simulations for absorptive perturbation $\Delta\mu_a/\mu_a$ ranging from -60% to 60% and the two time-resolved transmittance curves are almost indistinguishable. Discrepancies between FEM simulations and perturbation model predictions become evident with increasing radius of the inhomogeneity; the first-order perturbation model tends to underestimate the transmittance values, as it can be clearly seen in Fig. 3(b) where the radius is $R=10$ mm. In order to develop a more close comparison between the first-order perturbation model results and the FEM simulations, we have plotted in Fig. 4 the temporal dependence of the contrast functions $\delta T_{pert}(t)/T(t)$ and $\delta T_{num}(t)/T(t)$ for increasing values of the inhomogeneity radii and of the reduced scattering coefficient μ_s' of the host medium. The two functions are given by

$$\frac{\delta T_{pert}(t)}{T(t)}=\frac{T_{pert}(t)-T(t)}{T(t)}, \tag{26a}$$

$$\frac{\delta T_{num}(t)}{T(t)}=\frac{T_{num}(t)-T(t)}{T(t)}. \tag{26b}$$

The contrast function defined in Eq. (26a) in terms of the relative change in the perturbed transmittance signal, when the probe beam and the detector are aligned, is consistent with that used in Refs. [15,31]. Similarly, Eq. (26b) gives the relative change in the transmittance signal as obtained by the FEM simulation of the absorptive inclusion. The solid curves in Fig. 4 illustrate the temporal behavior of the contrast $\delta T_{num}(t)/T(t)$, employing the same slab geometry and absorption coefficient of the host medium as used to generate Fig. 3. The dashed curves are the predictions of the perturbed model $\delta T_{pert}(t)/T(t)$. Inspection of the curves shows that there is a significant enhancement of the contrast for increasing values of R and μ_s' over the temporal range of the transmitted signal and over the considered range of absorptive perturbation $\Delta\mu_a/\mu_a$. The discrepancies of the perturbation-model-based results remain within $\sim 20\%$ until $R\lesssim 5$ mm and $\mu_s'\lesssim 1\ \mathrm{mm}^{-1}$ and increase significantly for higher values of the scattering coefficient μ_s' and of the radius R of the inclusion. It is also clear from the numerical results that the perturbation model generally underestimates the contrast compared to the FEM simulation, the discrepancies for negative values of the absorptive perturbation $\Delta\mu_a/\mu_a$ being more marked than those corresponding to positive values. This behavior can be understood from the fact that in the former case the perturbed transmittance signal is higher contributing more to the contrast function. This can

also be appreciated from the plots of the temporal profiles of the transmittance curves shown in Fig. 3(b) for $\Delta\mu_a/\mu_a = -0.6$.

IV. ANALYSIS OF THE ACCURACY OF THE PERTURBATION MODEL AND DISCUSSION

The analytical model for the perturbed time-resolved transmittance $T_{pert}(t)$ as expressed by Eqs. (15) and (17) was implemented in a least square fitting procedure. This permitted the homogeneous slab solution $T(t)$ plus the absorptive perturbation $\delta T_{\mu_a}(t)$ to be fitted to a FEM simulation for a slab containing a Gaussian absorptive inclusion. This model always considers a single defect that has diameter $2R$ equal to the height h and that is placed at the center $z_{pc}=d/2$ of an otherwise homogeneous slab with thickness $d=40$ mm and refractive index mismatch $n=1.4$. The two parameters describing optically the host medium, the absorption and scattering coefficients, were obtained from the fit of $T(t)$ to the FEM simulation results in the case of the coaxial configuration without the absorptive cylindrical inclusion. Thus, in the fitting procedure of the perturbed transmittance, we allowed only the absorptive perturbation parameter $\Delta\mu_a$ to vary. We obtained meaningful results through the analysis of the fitted value $\Delta\mu_{a,fit}$ for different choices of the optical parameters of the host medium and for different values of the size R and $\Delta\mu_a$ parameter of the inhomogeneity. The linear least square fitting procedure [32,33] determines $\Delta\mu_{a,fit}$ by minimizing the χ^2 parameter defined as

$$\chi^2=\int_{t_{\min}}^{t_{\max}}\left(\frac{T_{pert}(t)-T_{num}(t)}{T_{num}(t)}\right)^2 dt, \tag{27}$$

where $T_{num}(t)$ is the time-resolved transmittance computed by the FEM simulation and the range of integration $[t_{\min},t_{\max}]$ depends on its temporal extent. The accuracy of the perturbation model can be quantitatively investigated by calculating the relative error $\epsilon_{\Delta\mu_a}$ defined as

$$\epsilon_{\Delta\mu_a}=\frac{\Delta\mu_a-\Delta\mu_{a,fit}}{\Delta\mu_a}, \tag{28}$$

which expresses the deviation of the fitted values $\Delta\mu_{a,fit}$ of the absorptive inclusion from the expected one, $\Delta\mu_a$. This error is basically a measure of the discrepancies between $T_{pert}(t)$ and $T_{num}(t)$ through the capability of the fitting procedure of recovering from the perturbed model $T_{pert}(t)$, the expected value $\Delta\mu_a$ of the absorption inclusion. Figures 5, 6, and 7 show the relative error $\epsilon_{\Delta\mu_a}$ as a function of the absorptive perturbation $\Delta\mu_a/\mu_a$ in the range -0.6 to 0.6 for three values of the reduced scattering coefficient μ_s', namely, $\mu_s'=0.5,1.0,1.5$ mm^{-1}, respectively. Each figure shows four panels corresponding to increasing values of the host absorption coefficient, $\mu_a=0.005,0.01,0.02,0.025$ mm^{-1}, and to four values of the radius R of the inclusion ranging from $R=2.5$ mm to $R=10$ mm. The relative error depends critically on the optical parameters of the host medium.

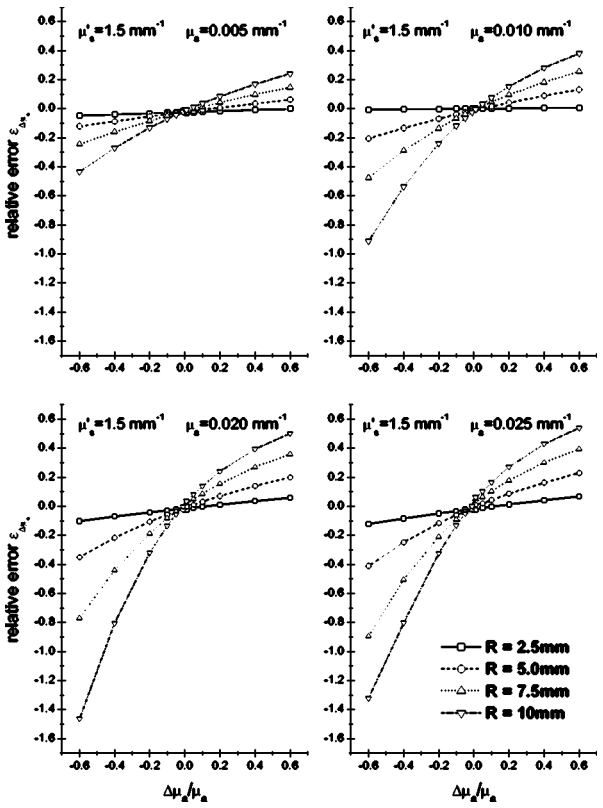

FIG. 7. Numerical calculation of the relative error $\epsilon_{\Delta\mu_a}$ as a function of the relative absorptive perturbation $\Delta\mu_a/\mu_a$ for $\mu_s'=1.5$ mm^{-1}. The four panels are obtained for increasing values (form top to bottom) of the absorption coefficient of the host medium: $\mu_a=0.005$, 0.01, 0.02, 0.025 mm^{-1}.

The general behavior that can be deduced from each figure is that the relative error increases with increasing the absorption coefficient for given values of μ_s', R, and $\Delta\mu_a/\mu_a$. This can be understood by taking into account the statistical weight factor $\exp\{-\int_0^l[\mu_a+\Delta\mu_a(\mathbf{r})]dl\}$, which describes the probability of survival of a photon following a trajectory of length l inside the region of the absorptive inclusion and which accounts for the decrease of the transmitted intensity. If we fix the value of the relative perturbation $\Delta\mu_a/\mu_a$ and consider increasing values of μ_a, the corresponding absorption perturbation $\Delta\mu_a$ increases, leading to a progressive reduction of the perturbed transmitted signal with respect to the unperturbed one and to a corresponding decrease of the accuracy of the perturbation model. It can also be seen that the relative error $\epsilon_{\Delta\mu_a}$ becomes higher for increasing values of the size R of the inclusion, as can be expected by considering that photon migration is more affected by higher values of the size of the inclusion and, consequently, the perturbation model predictions become less accurate. Another feature that can be deduced from the numerical results reported in the plots is the evident asymmetry of the relative error between positive and negative values of the relative absorptive perturbation $\Delta\mu_a/\mu_a$. The absolute values of the relative error are higher for negative values of $\Delta\mu_a/\mu_a$ as compared to those computed for positive values, a result that is consistent with our previous discussion on

discrepancies between the FEM-simulation-based contrast $\delta T_{num}(t)/T(t)$ and $\delta T_{pert}(t)/T(t)$ given in Eqs. (26a) and (26b). A photon passing through a positive absorptive inclusion has a higher probability of being absorbed compared to that traversing the same path in a negative absorptive inclusion, leading in the former case to a transmittance signal that deviates less with respect to the unperturbed one. Therefore, the fitting procedure is expected to be more accurate in the case of positive absorption inclusion. From the analysis of Figs. 5–7 it can also be clearly seen that the relative error increases with increasing the reduced scattering coefficient μ_s' of the surrounding medium. For a degree of the relative absorption perturbation $|\Delta\mu_a/\mu_a| \leqslant 20\%$, the relative error $\epsilon_{\Delta\mu_a}$ is less than 20% when the size of the inclusion is $R \leqslant 5$ mm in the considered range of the reduced scattering coefficient μ_s' and for absorption coefficient $\mu_a \leqslant 0.025\ \mathrm{mm}^{-1}$.

V. CONCLUSIONS

To summarize, we have performed a detailed analysis for the problem of photon migration through a scattering slab containing a single absorptive inclusion whose absorption coefficient is characterized by a Gaussian distribution in the radial direction. The analysis has been performed within the framework of the first-order perturbation approach to the diffusion theory for a slab geometry and a coaxial measurement arrangement. The proposed model can be used to describe the effect of an inclusion on light propagation through an otherwise homogeneous turbid medium for applications related to functional imaging. An analytical expression has been derived that accounts for the change in the time-resolved transmittance in presence of the absorptive Gaussian inclusion. The accuracy and the application range of the perturbed model has been investigated by comparing time-resolved transmittance profiles obtained by the perturbed expression with those obtained through the FEM simulations of the diffusion equation in presence of the inclusion. We have determined the relative error in recovering the absorption perturbation parameter of the inclusion by the fitting procedure. The analysis considered the case of absorptive inclusions located at the middle plane of the slab, since in this configuration the contrast functions attain their lower values. Sizes and optical parameters of the inclusion and host medium have been chosen so as to cover the range of values of practical interest in optical imaging of biological tissue. It has been shown that the perturbed model predictions become less accurate by increasing the size and the absorption coefficient of the inclusion and also by increasing the values of the optical coefficient of the host medium. The proposed perturbation model attains an accuracy better than 20% when the inclusion has a size less than 5 mm and the relative absorptive perturbation parameter $|\Delta\mu_a/\mu_a| \leqslant 20\%$ in the considered range of absorption and reduced scattering coefficient of the host medium. Furthermore, the FEM simulations have shown that the accuracy of the perturbation model is less than 10% for sizes of the inclusion less than 2.5 mm over the extended range of the absorptive perturbation $|\Delta\mu_a/\mu_a| \leqslant 60\%$.

[1] B. Chance, R.E. Alfano, and B.J. Tromberg, Proc. SPIE **3597** (1999).
[2] D. Grosenick, H. Wabnitz, H.H. Rinneberg, T. Moesta, and P.M. Schlag, Appl. Opt. **38**, 2927 (1999).
[3] M.A. Franceschini, K.T. Moesta, S. Fantini, G. Gaida, E. Gratton, H. Jess, W.W. Mantulin, M. Seeber, P.M. Schlag, and M. Kaschke, Proc. Natl. Acad. Sci. U.S.A. **94**, 6468 (1997).
[4] K. Gayen and R.R. Alfano, Opt. Photonics News **7**, 17 (1996).
[5] S. Ertefai and A.E. Profio, Med. Phys. **12**, 393 (1985).
[6] A.H. Gandjbakhche and G.H. Weiss, Phys. Rev. E **61**, 6958 (2000).
[7] M.P. VanAlbada and A. Lagendijk, Phys. Rev. Lett. **55**, 2692 (1985).
[8] A. Ishimaru (unpublished).
[9] D.A. Weitz, D.J. Pine, P.N. Pusey, and R.J.A. Tough, Phys. Rev. Lett. **63**, 1747 (1989).
[10] B.B. Das, K.M. Yoo, and R.R. Alfano, Opt. Lett. **18**, 1092 (1993).
[11] M.S. Patterson, B. Chance, and B.C. Wilson, Appl. Opt. **28**, 2331 (1989).
[12] S.R. Arridge, M. Cope, and D.T. Delpy, Phys. Med. Biol. **37**, 1531 (1992).
[13] J.C. Hebden and S.R. Arridge, Appl. Opt. **35**, 6788 (1996).
[14] G.H. Weiss and A.H. Gandjbakhche, Phys. Rev. E **56**, 3451 (1997).
[15] M. Morin, S. Verrealut, A. Mailloux, J. Fréchette, Y.P.S. Chatigny, and P. Beaudry, Appl. Opt. **39**, 2840 (2000).
[16] S. Carraresi, T.S.M. Shatir, F. Martelli, and G. Zaccanti, Appl. Opt. **40**, 4622 (2001).
[17] V.A. Markel and J. Schotland, Phys. Rev. E **64**, 035601 (2001).
[18] J.L. Karagiannes, B.G.Z. Zhang, and L.I. Grosswiner, Appl. Opt. **28**, 2311 (1989).
[19] M. Keijzer, W.M. Star, and P. Storchi, Appl. Opt. **27**, 1820 (1988).
[20] J.B. Fishkin, O. Coquoz, E.R. Anderson, M. Brenner, and B.J. Tromberg, Appl. Opt. **36**, 10 (1997).
[21] M. Keijzer, W.M. Star, and P.M. Storchi, Appl. Opt. **27**, 1820 (1988).
[22] R.C. Haskell, L.O. Svaasand, T.T. Tsay, C. Feng, M.S. McAdams, and B.J. Tromberg, J. Opt. Soc. Am. A **11**, 2727 (1994).
[23] D. Contini, F. Martelli, and G. Zaccanti, Appl. Opt. **36**, 4857 (1997).
[24] R. Aronson, J. Opt. Soc. Am. A **12**, 2532 (1995).
[25] M.R. Ostermeyer and S.L. Jacques, J. Opt. Soc. Am. A **14**, 255 (1997).
[26] J.M. Kaltenbach and M. Kaschke, Proc. SPIE **IS11**, 65 (1993).
[27] S.R. Arridge, Appl. Opt. **34**, 7395 (1995).
[28] S.R. Arridge, M. Schwieger, M. Hirakoa, and D.T. Delpy, Med. Phys. **20**, 299 (1993).
[29] M.S.S.R. Arridge, Appl. Opt. **34**, 8026 (1995).

[30] M. Shweiger, S.R. Arridge, M. Hiraoka, and D.T. Delpy, Med. Phys. **22**, 1779 (1995).
[31] Y. Painchaud, A. Mailloux, M. Morin, S. Verreault, and P. Beaudry, Appl. Opt. **38**, 3686 (1999).
[32] C. P. Library, CERN Computer Center Report No. CH-1211, 1993 (unpublished).
[33] M. R. F. James, CERN Computer Center Report No. CH-1211, 1983 (unpublished).